MODELING AND FIRST CHARACTERIZATION OF BROAD-SPECTRUM VIBRATION REJECTION OF FREQUENCY MODULATED GYROSCOPES

Marco Bestetti, Valentina Zega, and Giacomo Langfelder
Politecnico di Milano, Milano, ITALY

ABSTRACT

The work presents a detailed modeling and the first-ever characterization of a frequency modulated (FM) yaw gyroscope in presence of vibrations from low frequency (30 Hz), through the main modes, and up to 40 kHz. The gyroscope two in-plane axes (around 25 kHz) are operated under a Lissajous trajectory (70 Hz period) by an integrated circuit (IC) including oscillators, frequency digitization, and digital demodulation stages. In presence of 2-$g_{pk\text{-}pk}$ vibrations, no effects are visible across the spectrum apart from the region including the modes. In this range, as predicted by theory, for each axis no effect is observed for accelerations at the axis resonance (< 0.1 dps/g), but a huge effect (tens of dps/g) is visible for accelerations at an offset frequency from resonance corresponding to the mode split.

INTRODUCTION

The field of high-stability angular rate sensors is well debated and includes rejection of temperature effects [1], of aging [2], as well as of in-run vibrations [3]. The latter phenomenon may be the dominant factor affecting stability in certain harsh application fields like automotive. In recent years numerous studies on the topic have been presented in the literature, and corresponding strategies to minimize these effects were proposed. On one side, for amplitude-modulated (AM) gyroscopes, the most straightforward solution is to conceive a differential, levered structure [4], which, at the first order, compensate for all external forces acting on the suspended mass as a common mode (e.g. accelerations). Additionally, it has been shown and proved that the induced rate caused by accelerations decrease with drive amplitude; consequently, some effort was put in designing devices operated at a larger displacement (up to 12 µm). Combining these considerations, authors in [5] have shown a vibration error (a spurious change of the output) of less than 0.2 dps/g on a AM yaw differential structure.

On the other side, the endless request for ultra-stable gyroscope performances against temperature, associated with low manufacturing costs, led to the development of gyroscopes based on different working principles, which theoretically avoid the dependence of offset and scale factor over process and environmental parameters. Among others, a Lissajous frequency-modulated (FM) topology [6] with associated electronics was developed up to the digital output within sub-500-µA consumption [7, 8]. This sensor (shown in Fig. 1 aside its integrated circuit, IC) relies on the precession of the orbit of a suspended mass, kept simultaneously in oscillation along two orthogonal modes (ω_x, ω_y) at a slightly mismatch frequency. The resulting effect is an amplitude modulation of the FM signal, proportional to the applied rate and to a modal ratiometric parameter (α). FM gyroscopes operated under Lissajous mode have shown exceptional stability performances of offset (few °/h at more than 1000 s observation interval, see Fig. 2 [8]), and scale factor (few tens ppm/K [7]). This

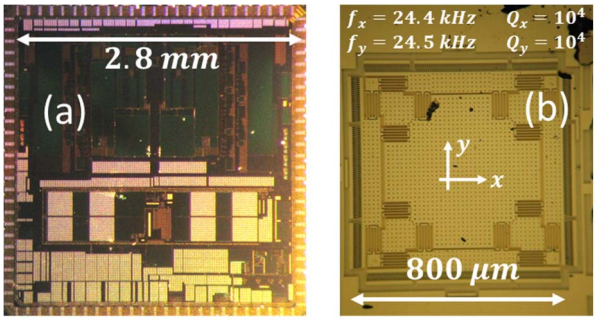

Fig. 1: optical microscope pictures of the developed integrated circuit (a) and of an uncapped Lissajous FM gyroscope (b), built in a 24-µm-thick MEMS process.

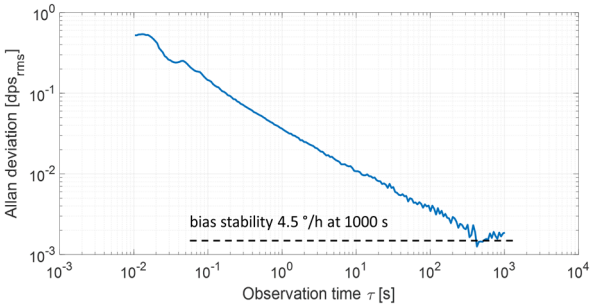

Fig. 2: measured Allan deviation of the FM gyroscope in uncontrolled laboratory environment, showing about 30 mdps/√Hz angle random walk and few °/h bias stability at 1000 s of observation interval.

paper further investigates stability by modeling and testing the FM gyroscope system of Fig. 1 under broad-spectrum vibrations. In the literature this key aspect is indeed missing.

The manuscript is organized as follows: exhaustive analytical equations are presented in the next section, together with simulation results of a Simulink behavioral model, which proves their validity. Then, the setup used for the measurements is described and finally the measurement results are discussed and compared to predictions.

MODEL DESCRIPTION

Notation

Along the manuscript the following notation is adopted.

x, y	*x- and y-direction displacement*
x_a, y_a	*amplitude of sinusoidal displacement x, y*
a_x, a_y	*x- and y-axis external acceleration*
a_{xa}	*amplitude of sinusoidal acceleration a*
m_x, m_y	*x- and y-axis modal mass*
k_x, k_y	*x- and y-axis stiffness*
b_x, b_y	*x- and y-axis damping coefficient*
ω_x, ω_y	*x- and y-axis resonance frequency*
$\omega_\Delta = \omega_x - \omega_y$	*frequency split*
F_x, F_y	*electrostatic drive force*
F_{xa}, F_{ya}	*amplitude of sinusoidal forces F_x, F_y*
Ω	*angular rate*

Table 1. Table of used parameters.

Analytical model

The examined phenomenon has first been modeled with an analytical approach. The starting point is the well-known system of coupled dynamic equations of a gyroscope, which comprises all the forces acting on the proof mass in both x- and y-direction. The external vibration is here supposed to occur along the x-direction, consistently with the measurements later discussed in the corresponding section of this manuscript.

$$\begin{cases} m_x\ddot{x} + b_x\dot{x} - 2\alpha m_x\Omega_z\dot{y} + k_x x = F_x + m_x a_x \\ m_y\ddot{y} + b_y\dot{y} + 2\alpha m_y\Omega_z\dot{x} + k_y y = F_y \end{cases} \quad (1)$$

For the purpose of this research, one can ignore cross-stiffness and cross-damping terms [9]. One can pass to a phasor description as indicated by Eqs (2):

$$\begin{cases} x = x_a e^{j\omega_x t} \\ y = y_a e^{j\omega_y t} = y_a e^{j(\omega_x - \omega_\Delta)t} \\ F_x = jF_{xa}e^{j\omega_x t} \\ F_y = jF_{ya}e^{j\omega_y t} \\ a_x = a_{xa}e^{j[(\omega_x - \omega_{\Delta\mathrm{ax}})t + \phi_{0,ac}]} \\ a_y = 0 \end{cases} \quad (2)$$

Since the goal is to derive the expression of the resonance frequency and its dependence on the acceleration, both equations are divided by the displacement after substituting Eq. 2 into Eq. 1. This is shown by Eq. 3 at the bottom of the page. The analysis continues using the Euler identity and focuses on the real part of both equations (Eq. 4).

A further simplification can be done assuming an ideal amplitude control ($x_a = y_a$) and linearizing the equations assuming that the natural frequency of each mode is much greater than the amplitude of the two terms given by the rate and the accelerations, Eq. 5. The obtained result shows that, as expected, the rate is modulated at the frequency split between the two axes. Accelerations (a_{xa}) are instead divided by the velocity amplitude ($\omega_{0x}x_a$) and modulated at a frequency corresponding to the difference $\omega_{\Delta\mathrm{ax}}$ between the acceleration frequency and the resonance frequency of the considered axis. Therefore, if the acceleration occurs at the resonance frequency ω_x, this term becomes a DC contribution, which goes out of the sensor bandwidth after the AM demodulation. Interestingly instead, if the acceleration occurs at a frequency which is split from the resonance by the same quantity of the mode split (or lies at a distance within the bandwidth from this value), an effect of the acceleration on the frequency should be well visible. Its amplitude randomly depends on the phase $\phi_{0,ac}$ of the acceleration term relative to the phase of the Lissajous pattern. Note that this effect occurs even in presence of amplitude control in the oscillators, since it is not trivial to implement a large-bandwidth amplitude control, i.e. with a high loop-gain and 180°-phase at the mismatch frequency [10].

Far from the modes, no effect should be visible as the acceleration-induced signal lies well off the bandwidth set by the low-pass filter after the amplitude demodulation.

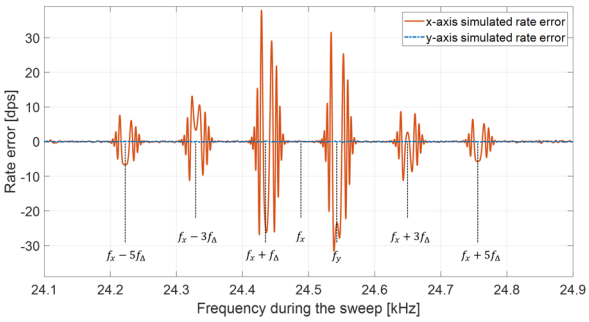

Fig. 3: behavioral model showing the rate error induced by an x-axis acceleration occurring at frequencies in the range of the two modes.

Simulink and MATLAB behavioral

The proposed analytical computation agrees with a Simulink behavioral model of the entire system, composed by the FM gyroscope, two analog oscillators, two frequency-to-digital stages and a digital demodulation.

The applied acceleration in the simulation testbench has a constant amplitude and a varying frequency with time. The purpose is to simulate the frequency response of the FMG-system with an analysis performed in the time domain. Fig. 3 shows a detail of the x-axis output (in terms of input-referred angular rate) when the acceleration frequency sweeps over the range that includes the two sensor modes of interest. As predicted by Eq. (5) no effects are visible when $\omega_{\Delta ax}$= 0, i.e. when the frequency of the

$$\begin{cases} -\omega_x^2 + \dfrac{jb_x\omega_x}{m_x} - j2\Omega_z\omega_y\dfrac{y_a}{x_a}e^{-j\omega_\Delta t} + \dfrac{k_x}{m_x} = \dfrac{jF_{xa}}{x_a m_x} + \dfrac{a_{xa}}{x_a}e^{-j[\omega_{\Delta\mathrm{ax}}t + \phi_{0,ac}]} \\ -\omega_y^2 + \dfrac{jb_y\omega_y}{m_y} + j2\Omega_z\omega_x\dfrac{x_a}{y_a}e^{j\omega_\Delta t} + \dfrac{k_y}{m_y} = j\dfrac{F_{ya}}{y_a m_y} \end{cases} \quad (3)$$

$$\begin{cases} \omega_x^2 = -2\Omega_z\omega_y\dfrac{y_a}{x_a}sin(\omega_\Delta t) + \dfrac{k_x}{m_x} + \dfrac{a_{xa}}{x_a}cos(\omega_{\Delta ax}t + \phi_{0,ac}) \\ \omega_y^2 = -2\Omega_z\omega_x\dfrac{x_a}{y_a}sin(\omega_\Delta t) + \dfrac{k_y}{m_y} \end{cases} \quad (4)$$

$$\begin{cases} \omega_x = \omega_{0x} - \Omega_z sin(\omega_\Delta t) + \dfrac{a_{xa}}{2\omega_{0x}x_a}\cos(\omega_{\Delta\mathrm{ax}}t + \phi_{0,ac}) \\ \omega_y = \omega_{0y} - \Omega_z sin(\omega_\Delta t) \end{cases} \quad (5)$$

acceleration is equal to the resonance frequency ω_x of the x-axis, excited by the acceleration. A variable response (depending on the random phase difference between the acceleration and the oscillation) is instead visible for $\omega_{\Delta ax} = \omega_\Delta$ i.e. when the frequency of the acceleration is equal to the resonance frequency ω_y of the y-axis (not excited by the acceleration). In general, an erroneous rate appears also for accelerations occurring at a frequency distance from ω_y within the bandwidth of the sensor. In addition, a similar effect is visible for the odd order harmonics of the mismatch, this being caused by the square-wave amplitude demodulation.

MEASUREMENTS RESULTS

The yaw FM gyroscope is first characterized under rotational rates: it shows a combined ratiometric scale-factor of 1.6 Hz/Hz and a 4.5 °/h stability (Fig. 2).

Fig. 4 shows the used setup for the vibration tests: the gyroscope is glued on top of the IC, in turn glued on a ceramic carrier. Electrical connections are obtained through bonding wires. The carrier is placed on a printed circuit board which brings the signal to an external digital acquisition board. The system is mounted on the shaker, capable of generating wide-spectrum vibrations up to few g-units of acceleration. The orientation of the board is such that vibrations occur along one of the modes of interest (the x-axis mode), for an initial validation of the proposed model. The applied vibration amplitude is controlled in feedback by an auxiliary piezoelectric accelerometer. Vibrations are swept in time from low frequency (30 Hz, the minimum applicable by the setup) to almost 40 kHz. Portions of this range should be avoided due to the presence of setup modes.

Experimental measurements confirm the model predictions over a broad spectrum, showing (i) no effects

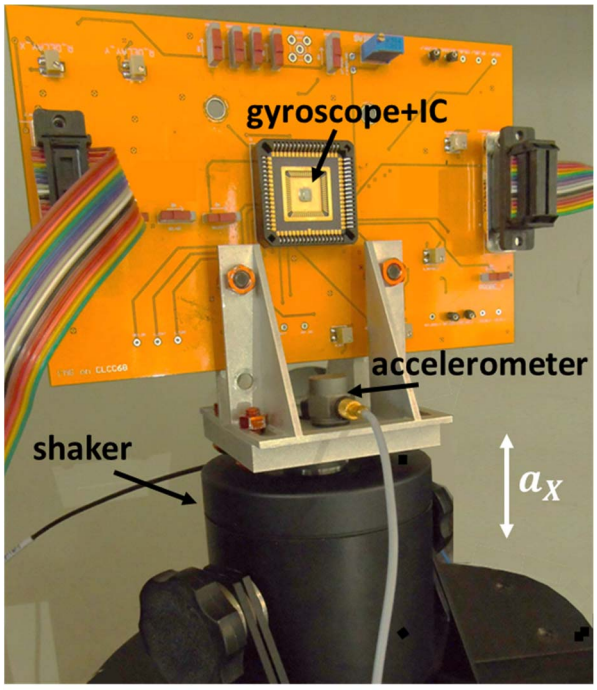

Fig. 4: picture of the setup including a mini-shaker with a reference accelerometer, aligned below the MEMS and IC (glued on a carrier), along the vibration axis (corresponding to the gyroscope x-axis in this case).

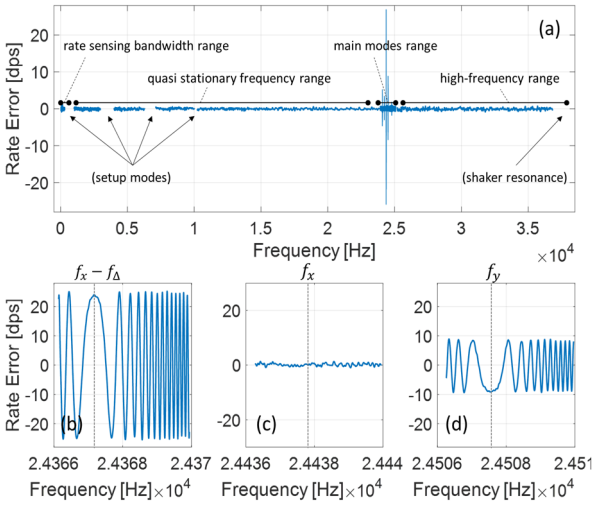

Fig. 5: (a) measured system output under accelerations from 30 Hz to 40 kHz (2-$g_{pk\text{-}pk}$). As predicted by the developed theory, and according to the behavioral model, effects are observed only at a frequency split (and its odd harmonics) from the axis frequency (b, d), with amplitude randomness given by the acceleration phase $\Phi_{0,ac}$ relative to the split phase $\omega_\Delta \cdot t$. No effect for the x-axis output is visible for an acceleration at its resonance frequency (c).

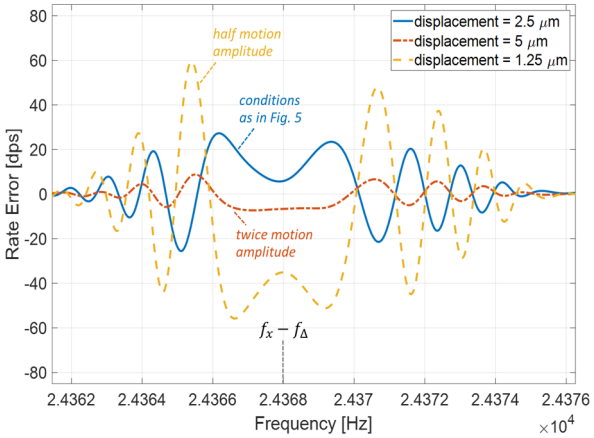

Fig. 6: effects of oscillation amplitude changes on the rate error caused by vibrations. As predicted by theory, doubling the motion amplitude from 2.5 µm to 5 µm halves the rate error down to 8 dps/g.

across the spectrum far from the modes (Fig. 5a, left range), (ii) no effects for accelerations at the resonance frequency of the excited x-axis (Fig. 5c), but (iii) evident random effects (up to 20 dps/g, depending on the random acceleration phase) for accelerations occurring at the other-axis frequency or up to a distance from it equal to the mode split (see the zooms in Fig. 5b and 5d).

Finally, measurements at different amplitudes of oscillation along the two gyroscope axes are presented in Fig. 6. Here only the frequency range around $\boldsymbol{\omega_y}$ is shown (corresponding to subfigure b of Fig. 5). As predicted by theory (Eq. 5), doubling the motion amplitude from 2.5 µm to 5 µm halves the spurious rate error down to 8 dps/g. On the contrary, halving the controlled motion amplitude by a factor 2 implies a heavier effect of vibrations by the same factor. The obtained values are in general larger than corresponding values for tuning-fork-based amplitude modulated gyroscopes.

CONCLUSIONS

The presented considerations and evidences on rejection of external vibrations highlight a so far unconsidered issue for this class of sensors and push for the development of FM gyroscopes with either higher operating modes [11] and/or larger displacement.

Another viable option is the implementation of more sophisticated structures with improved vibration rejection capabilities. In analogy with AM gyroscopes, the development of two-mass structures could be beneficial. These structures have already been demonstrated for the LFM gyroscope topology [12], and in the future they will be tested under vibration disturbances to validate their effective robustness on this side. Similarly, quad-mass devices, already proposed in the literature [13, 14], will be investigated as alternative options – at the cost of an increased sensor footprint.

If not mitigated, the effects discussed in this work may jeopardize the benefits in terms of stability that Lissajous FM gyroscopes have demonstrated in previous works.

REFERENCES

[1] E. Tatar, C. Guo, T. Mukherjee and G. K. Fedder, "Interaction effects of temperature and stress on matched-mode gyroscope frequencies," 2013 Transducers & Eurosensors *in proc. TRANSDUCERS & EUROSENSORS XXVII*, Barcelona, 2013, pp. 2527-2530.

[2] S. Nadig and A. Lal, "In-situ calibration of MEMS inertial sensors for long-term reliability," *2018 IEEE International Reliability Physics Symposium (IRPS)*, Burlingame, CA, 2018, pp. 3C.8-1-3C.8-4.

[3] S. W. Yoon, S. W. Lee, N. C. Perkins and K. Najafi, "Vibration Sensitivity of MEMS Tuning Fork Gyroscopes," *SENSORS, 2007 IEEE*, Atlanta, GA, 2007, pp. 115-119.

[4] F. Giacci, S. Dellea, A. F. Longoni and G. Langfelder, "Vibrations rejection in gyroscopes based on piezoresistive nanogauges," *18th International Conference on Solid-State Sensors, Actuators and Microsystems (TRANSDUCERS)*, Anchorage, AK, 2015, pp. 780-783.

[5] L. G. Pagani, S. Dellea, G. Bursi, M. Brunetto, L. Falorni and G. Langfelder, "Enhancing Vibration Robustness and Noise in Automotive Gyroscope with Large Drive Motion and Levered Sense Mode," *2019 IEEE MEMS*, Seoul, South Korea, 2019, pp. 708-711.

[6] I. I. Izyumin et al., "A 7ppm, 6°/hr frequency-output MEMS gyroscope," *28th IEEE International Conference on Microelectromechanical Systems (MEMS)*, Estoril, 2015, pp. 33-36.

[7] P. Minotti et al., "High Scale-Factor Stability Frequency-Modulated MEMS Gyroscope: 3-Axis Sensor and Integrated Electronics Design," *IEEE Transactions on Industrial Electronics*, vol. 65, no. 6, pp. 5040-5050, June 2018.

[8] M. Leoncini, M. Bestetti, A. Bonfanti, S. Facchinetti, P. Minotti and G. Langfelder, "Fully Integrated, 406 µA, 5°/hr, Full Digital Output Lissajous Frequency-Modulated Gyroscope," *IEEE Transactions on Industrial Electronics*, vol. 66, no. 9, pp. 7386-7396, Sept. 2019.

[9] E. Tatar, S. E. Alper and T. Akin, "Quadrature-Error Compensation and Corresponding Effects on the Performance of Fully Decoupled MEMS Gyroscopes," *Journal of Microelectromechanical Systems*, vol. 21, no. 3, pp. 656-667, June 2012.

[10] B. Eminoglu and B. E. Boser, "Chopped rate-to-digital FM gyroscope with 40ppm scale factor accuracy and 1.2dph bias," *2018 IEEE International Solid - State Circuits Conference - (ISSCC)*, San Francisco, CA, 2018, pp. 178-180.

[11] A. Rahafrooz, D. E. Serrano, D. Younkin, S. Nagpal, I. Jafri and F. Ayazi, "A 0.5 mm^2 7-MHz capacitive bulk acoustic wave gyroscope in (100) silicon with large dynamic range," *IEEE 30th International Conference on Micro Electro Mechanical Systems (MEMS)*, Las Vegas, NV, 2017, pp. 25-28.

[12] V. Zega *et al.*, "A dual-mass frequency-modulated (FM) pitch gyroscope: Mechanical design and modelling," *2018 IEEE International Symposium on Inertial Sensors and Systems (INERTIAL)*, Moltrasio, 2018, pp. 1-4.

[13] S. Askari, M. H. Asadian, K. Kakavand and A. M. Shkel, "Vacuum sealed and getter activated MEMS Quad Mass Gyroscope demonstrating better than 1.2 million quality factor," *2016 IEEE International Symposium on Inertial Sensors and Systems*, Laguna Beach, CA, 2016, pp. 142-143.

[14] J. Chen, T. Tsukamoto and S. Tanaka, "Quad Mass Gyroscope with 16 ppm Frequency Mismatch Trimmed by Focus Ion Beam," *2019 IEEE International Symposium on Inertial Sensors and Systems (INERTIAL)*, Naples, FL, USA, 2019, pp. 1-4.